基于热力学模拟的碱激发材料物相演变与耐久性能研究进展

Zuo, Yibing; Liao, Yishun; Yang, Yingzi; Ye, Guang

DOI
10.14062/j.issn.0454-5648.20230323

Publication date
2024

Document Version
Final published version

Published in
Kuei Suan Jen Hsueh Pao/Journal of the Chinese Ceramic Society

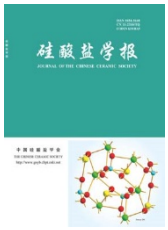

硅酸盐学报
Journal of the Chinese Ceramic Society
ISSN 0454-5648,CN 11-2310/TQ

《硅酸盐学报》网络首发论文

题目：基于热力学模拟的碱激发材料物相演变与耐久性能研究进展
作者：左义兵，廖宜顺，杨英姿，叶光
DOI：10.14062/j.issn.0454-5648.20230323
收稿日期：2023-05-12
网络首发日期：2023-12-04
引用格式：左义兵，廖宜顺，杨英姿，叶光．基于热力学模拟的碱激发材料物相演变与耐久性能研究进展[J/OL]．硅酸盐学报．
https://doi.org/10.14062/j.issn.0454-5648.20230323

网络首发时间：2023-12-04 17:22:26
网络首发地址：https://link.cnki.net/urlid/11.2310.TQ.20231201.1158.005

http://www.gxyb.cbpt.cnki.net　　DOI：10.14062/j.issn.0454-5648.20230323

综 合 评 述

基于热力学模拟的碱激发材料物相演变与耐久性能研究进展

左义兵[1,2]，廖宜顺[3]，杨英姿[4]，叶　光[5]

(1. 华中科技大学土木与水利工程学院，武汉 430074；2. 国家环境保护矿冶资源利用与污染控制重点实验室，武汉 430081；3. 武汉科技大学城市建设学院，武汉 430065；4. 哈尔滨工业大学土木工程学院，哈尔滨 150090；5. 代尔夫特理工大学土木与地球科学学院，荷兰 代尔夫特 2628CN)

摘　要：热力学模拟是研究碱激发材料化学反应的有效方法，对于深入研究和探明碱激发材料物相演变规律与耐久性能具有重要意义。本文从热力学模拟的基本原理出发，介绍了碱激发材料的热力学数据库以及热力学模拟方法，分析和总结了热力学模拟在碱激发材料反应机理、侵蚀性介质作用下物相演变规律、耐久性能和原材料组成设计等研究中的应用进展，指出了现阶段碱激发材料领域热力学模拟研究存在的不足并提出了展望，为基于热力学模拟的碱激发材料研究提供理论指导。

关键词：碱激发材料；物相演变；耐久性能；热力学数据库；热力学模拟
中图分类号：TU526　　**文献标志码：**A　　**文章编号：**0454–5648(2024)02–0000–12

碱激发材料(AAMs)是由含有铝硅酸盐的前驱体(如矿渣、粉煤灰和偏高岭土等)与碱性溶液(如氢氧化钠、硅酸钠和碳酸钠等)反应生成的一种具有特殊性能的新型绿色胶凝材料[1–3]，不仅可以降低能源和矿产资源消耗、减少二氧化碳排放[4–5]，而且具备早强快硬、耐酸碱盐腐蚀等特点[6–7]。显然，碱激发材料是原材料经过一系列化学反应而形成的具有一定胶凝能力的材料。因此，反应前的原材料组成与反应后的产物类型、孔溶液化学组成是影响碱激发材料物相演变和耐久性能的重要因素。

碱激发材料前驱体来源丰富，不同来源的前驱体化学性质(如化学组成、反应活性以及活性组分含量等)和物理性质(如比表面积和粒径分布等)存在显著差异，而碱性激发剂也存在多样性，包括碱(如氢氧化钠和氢氧化钾等)和溶解呈碱性的盐(如硫酸钠和碳酸钠等)[8–10]。此外，相比于普通硅酸盐水泥较为确定的矿物组成(C_2S、C_3S、C_3A 和 C_4AF)及其水化反应，前驱体活性组分的矿物组成和活性大小并不确定，关于活性组分参与的化学反应也尚未明确。

根据前驱体活性组分中钙含量和主要反应产物特点，一般将碱激发材料分为碱激发高钙、低钙和中钙体系[8, 11]，其中：碱激发高钙体系以碱激发矿渣为代表，主要反应产物为 C-(N-)A-S-H 凝胶；碱激发低钙体系以碱激发粉煤灰和偏高岭土为代表，主要反应产物为 N-A-S-H 凝胶；碱激发中钙体系以碱激发矿渣-粉煤灰复合胶凝材料为代表，主要反应产物为 C-(N-)A-S-H 凝胶与 N-A-S-H 凝胶共存。碱激发材料次要反应产物种类繁多，不仅取决于前驱体类型和组成，还受碱激发剂类型和养护条件的影响[12–13]。

由于碱激发剂的引入，碱激发材料孔溶液比硅酸盐水泥体系孔溶液含有更加丰富的离子，如钠离子、氢氧根离子和硅酸根离子等[14–15]。复杂的孔溶液化学组成不仅影响碱激发材料化学反应的热力学过程[16–17]和动力学过程[18–19]，而且影响碱激发材料的耐久性[20–21]。

此外，碱激发材料原材料组成、反应产物和孔溶液并非相互独立，而是相互影响，使得碱激发材料反应过程和性能演变更为复杂。因此，采用合适的研究方法对于探明碱激发材料物相演变规律和耐久性能尤为重要。近些年来，越来越多学者开始采用热力学模拟等数值方法来研究碱激发材料，取得了丰硕研究成果[17, 22–24]。

收稿日期：2023–05–12。　修订日期：2023–08–09。
基金项目：湖北省自然科学基金(2022CFB048)；国家环境保护矿冶资源利用与污染控制重点实验室(HB202103)。
第一作者：左义兵(1986—)，男，博士，讲师。

Received date: 2023–05–12.　**Revised date:** 2023–08–09.
First author: ZUO Yibing (1986–), male, Ph.D., Lecturer.
E-mail: zuoyibing@hust.edu.cn

热力学模拟能够根据碱激发材料原材料组成和给定反应条件，预测化学反应引起的反应产物和孔溶液变化，为研究碱激发材料物相变化和性能演变规律提供了有效技术途径。本文将从热力学模拟的基本原理出发，介绍碱激发材料化学反应的热力学数据库和热力学模拟方法，分析和总结国内外关于碱激发材料领域热力学模拟的研究现状和发展趋势，并梳理当前热力学模拟研究仍待解决和亟需关注的问题，为基于热力学模拟的碱激发材料研究提供指导。

1　热力学模拟的基本原理

碱激发材料中的化学反应遵循热力学定律。图 1 是碱激发材料中化学反应的热力学示意图。当铝硅酸盐前驱体与碱激发剂溶液接触时，其组分开始溶解，导致溶液中离子浓度增加(虚线所示)。当离子浓度增加到一定程度，使溶液中反应产物离子达到饱和或过饱和时，这些离子在热力学上更易于沉淀并生成反应产物。因此，这些离子的浓度开始下降。随后，系统中存在两种热力学相互作用：一种是前驱体和溶液之间的热力学相互作用，通过溶解不断将组成元素释放到溶液中；另一种是溶液和反应产物之间的热力学相互作用，使得反应产物不断增加。这两种热力学相互作用最终在液相和固相之间趋于热力学平衡，在这个过程中，铝硅酸盐前驱体逐渐向反应产物转化。

基于一定的前驱体反应度以及溶液与反应产物之间处于热力学平衡的假设，热力学模拟研究的基本过程如图 2 所示。基于样品参数输入，结合热力学数据库和热力学计算软件，通过热力学计算得到系统处于平衡状态时的反应产物组成和液相化学组成。在给定条件下，热力学模拟结果的准确性和可靠性需要丰富、准确的热力学数据库来保证。热力学数据库由所有固相、液相和气相的热力学参数组成，包括溶度积常数(K_{sp})、热容量(C_p^{Θ})、熵(S^{Θ})、Gibbs 自由能变($\Delta_f G_m^{\Theta}$)、焓变($\Delta_f H^{\Theta}$)和摩尔体积(V^{Θ})。由于热力学只关注反应的始态和终态，而反应的中间产物没有考虑，因此本文调研的所有热力学模拟研究结果展现的都是给定反应条件下的稳态反应产物。

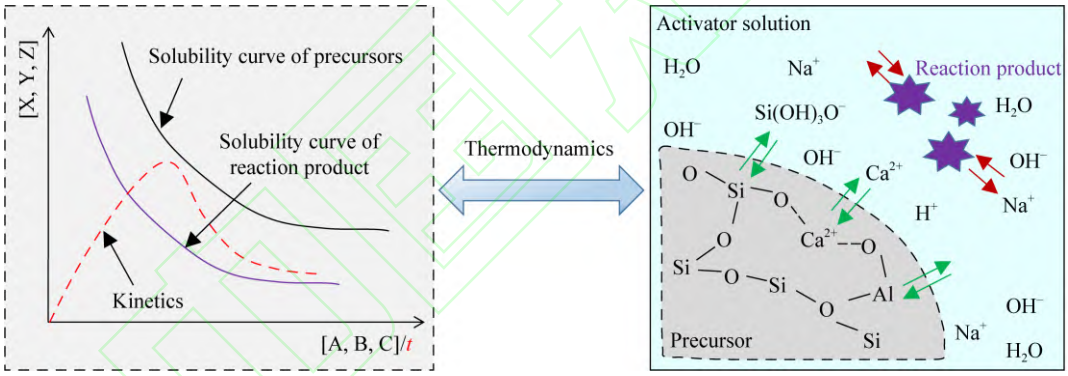

[X, Y, Z] and [A, B, C] represent the concentrations of aqueous ions X, Y, Z and A, B, C, respectively; *t* is time.

图 1　碱激发材料化学反应的热力学分析示意图

Fig. 1　An illustration of thermodynamics in AAMs

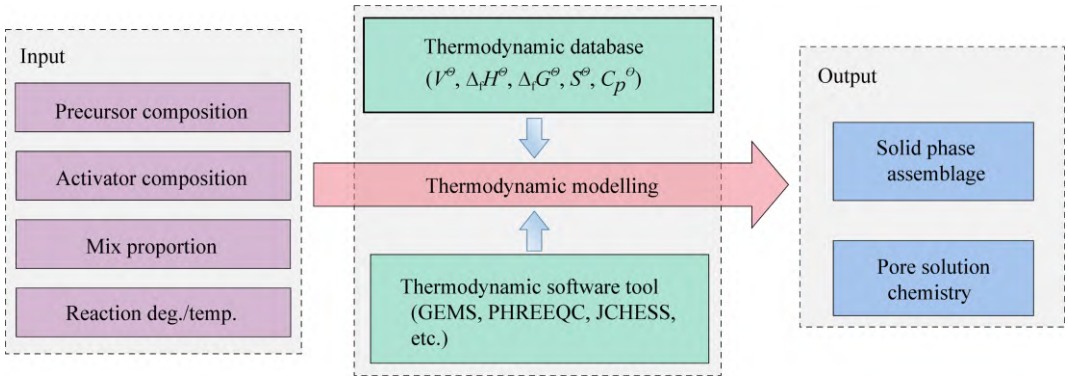

图 2　热力学模拟的基本过程

Fig. 2　An illustration of the thermodynamic modelling scheme

2　碱激发材料的热力学数据库

碱激发材料的热力学数据库通常以硅酸盐水泥体系的热力学数据库为基础，通过引入碱激发材料特有反应产物相而建立。表 1 列出了碱激发矿渣(高钙体系)、碱激发粉煤灰(低钙体系)和普通硅酸盐水泥的反应产物[25]，其中 C-(N-)A-S-H 凝胶和 N-A-S-H 凝胶分别是碱激发高钙体系和碱激发低钙体系区别于硅酸盐水泥体系所特有的反应产物。在碱激发中钙体系中，碱激发高钙体系和碱激发低钙体系的反应产物均有可能生成，例如：在碱激发矿渣-粉煤灰复合胶凝材料中，C-(N-)A-S-H 凝胶和 N-A-S-H 凝胶共存[26–28]；此外，城市固体废弃物焚烧(MSWI)底灰作为一种中钙含量的前驱体，研究者在碱激发 MSWI 底灰中也发现了 C-(N-)A-S-H 凝胶和 N-A-S-H 凝胶共存[29–30]。因此，建立碱激发材料特有反应产物相的热力学模型并确定其热力学参数，是建立相应热力学数据库的关键。

2.1　碱激发高钙体系的热力学数据库

C-(N-)A-S-H 凝胶是碱激发高钙体系特有的反应产物，建立其热力学模型并确定其热力学参数是建立碱激发高钙体系热力学数据库的关键。研究发现，C-(N-)A-S-H 凝胶与 C-S-H 凝胶结构类似，都是二维层状结构[31]。基于此，Myers 等[32]从 C-S-H 凝胶的结构模型出发，考虑碱激发高钙体系中 Al 和 Na 对凝胶结构和组成的影响，建立了描述 C-(N-)A-S-H 凝胶的热力学模型 CNASH_ss 并确定了其热力学参数。CNASH_ss 模型由 8 个凝胶单元组成，其分解反应见表 2，具体的热力学参数可参考文献[32]。此外，研究发现普通硅酸盐水泥体系热力学数据库中含氢氧根水滑石的热力学参数，并不能很好描述碱激发高钙体系中含氢氧根水滑石的生成[33]。为此，Myers 等[33]进一步建立了描述碱激发高钙体系中含氢氧根水滑石的热力学模型 MgAl-OH-LDH_ss，其分解反应见表 3，具体的热力学参数可参考文献[33]。基于硅酸盐水泥体系的热力学数据库，通过引入 CNASH_ss 和 MgAl-OH-LDH_ss 模型及其热力学参数，即可建立碱激发高钙体系的热力学数据库。目前，2018 年发布的热力学数据库 Cemdata18 已经包含了 CNASH_ss 和 MgAl-OH-LDH_ss 模型及其热力学参数[34]，可以直接用来对碱激发高钙体系进行热力学模拟研究。

2.2　碱激发低钙体系的热力学数据库

N-A-S-H 凝胶是碱激发低钙体系特有的反应产物，建立其热力学模型并确定其热力学参数是建立碱激发低钙体系热力学数据库的关键。相比于

表 1　碱激发材料和普通硅酸盐水泥的反应产物[25]

Table 1　Reaction products of AAMs and ordinary Portland cement (OPC) based materials[25]

Reaction products	OPC	AAMs	
		Alkali-activated slag	Alkali-activated fly ash
Primary	C-S-H	C-(N-)A-S-H	N-A-S-H
Secondary	CH, AFm, AFt	Hydrotalcite, C_4AH_{13}, C_2ASH_8, C_4AcH_{11}, $C_8Ac_2H_{24}$	Hydroxysodalite, Na-chabazite, faujasite, zeolite P ($N_3A_3S_{14}H_{15}$), zeolite Y (NAS_4H_8)

Notations: C=CaO, S=SiO_2, A=Al_2O_3, N=Na_2O, H=H_2O, c=CO_2, AFm=monosulfate aluminate hydrate, AFt=ettringite

表 2　CNASH_ss 模型的分解反应及其溶度积常数(298.15 K)[32]

Table 2　Dissociation reactions and solubility products of CNASH_ss (298.15 K)[32]

Solids	Molar ratios		Dissociation reactions	$\lg(K_{sp}^{\Theta})$
	Ca/Si	Al/Si		
5CA	1.25	0.25	$(CaO)_{1.25}\cdot(Al_2O_3)_{0.125}\cdot(SiO_2)\cdot(H_2O)_{1.625}\leftrightarrow 1.25Ca^{2+}+SiO_3^{2-}+0.25AlO_2^-+0.25OH^-+1.5H_2O$	–10.75
INFCA	0.84	0.26	$(CaO)\cdot(Al_2O_3)_{0.15625}\cdot(SiO_2)_{1.1875}\cdot(H_2O)_{1.65625}+0.687\,5OH^-\leftrightarrow Ca^{2+}+1.187\,5SiO_3^{2-}+0.312\,5AlO_2^-+2H_2O$	–8.90
5CNA	1.25	0.25	$(CaO)_{1.25}\cdot(Na_2O)_{0.25}\cdot(Al_2O_3)_{0.125}\cdot(SiO_2)\cdot(H_2O)_{1.25}\leftrightarrow 1.25Ca^{2+}+SiO_3^{2-}+0.25AlO_2^-+0.5Na^++0.75OH^-+H_2O$	–10.40
INFCNA	0.84	0.26	$(CaO)\cdot(Na_2O)_{0.34375}\cdot(Al_2O_3)_{0.15625}\cdot(SiO_2)_{1.1875}\cdot(H_2O)_{1.3}\leftrightarrow Ca^{2+}+1.187\,5SiO_3^{2-}+0.312\,5AlO_2^-+0.687\,5Na^++1.312\,5H_2O$	–10.00
INFCN	0.67	0	$(CaO)\cdot(Na_2O)_{0.3125}\cdot(SiO_2)_{1.5}\cdot(H_2O)_{1.1875}+0.375OH^-\leftrightarrow Ca^{2+}+1.5SiO_3^{2-}+0.625Na^++1.375H_2O$	–10.70
T2C*	1.50	0	$(CaO)_{1.5}\cdot(SiO_2)\cdot(H_2O)_{2.5}\leftrightarrow 1.5Ca^{2+}+SiO_3^{2-}+OH^-+2H_2O$	–11.60
T5C*	1.00	0	$(CaO)_{1.25}\cdot(SiO_2)_{1.25}\cdot(H_2O)_{2.5}\leftrightarrow 1.25Ca^{2+}+1.25SiO_3^{2-}+2.5H_2O$	–10.50
TobH*	0.67	0	$(CaO)\cdot(SiO_2)_{1.5}\cdot(H_2O)_{2.5}\leftrightarrow Ca^{2+}+1.5SiO_3^{2-}+3H_2O$	–7.90

*It indicates that these components have the same bulk chemistry but slightly modified thermodynamic properties relative to the T2C, T5C and TobH end-members of the downscaled CSH3T model[32].

表 3 MgAl-OH-LDH_ss 模型的分解反应及其溶度积常数(298.15 K)[33]

Table 3 Dissociation reactions and solubility products of MgAl-OH-LDH_ss (298.15K)[33]

Solids	Mg/Al	Dissociation reactions	$\lg(K_{sp}^{\Theta})$
$(MgO)_4\ (Al_2O_3)\ (H_2O)_{10}$	2	$Mg_4Al_2(OH)_{14}(H_2O)_3 \leftrightarrow 4Mg^{2+}+2AlO_2^-+6OH^-+7H_2O$	–49.70
$(MgO)_6\ (Al_2O_3)\ (H_2O)_{12}$	3	$Mg_6Al_2(OH)_{18}(H_2O)_3 \leftrightarrow 6Mg^{2+}+2AlO_2^-+10OH^-+7H_2O$	–72.02
$(MgO)_8\ (Al_2O_3)\ (H_2O)_{14}$	4	$Mg_8Al_2(OH)_{22}(H_2O)_3 \leftrightarrow 8Mg^{2+}+2AlO_2^-+14OH^-+7H_2O$	–94.34

C-(N-)A-S-H 凝胶，N-A-S-H 凝胶的热力学研究鲜有报道，这是因为 N-A-S-H 凝胶是一种结构无序和高度交联的三维网状结构[35]，其结构和化学组成因前驱体组成和碱激发条件的不同而存在显著差异[12–13]，目前定量描述 N-A-S-H 凝胶的结构模型还未见报道。

尽管 N-A-S-H 凝胶长程无序，但研究发现其在 8 Å 长度范围内的局部结构有序，且与白榴石晶体结构类似[36–37]。因此，Zuo 等[38]以白榴石为基准，参考已有关于 N-A-S-H 凝胶化学组成的文献报道，建立了描述 N-A-S-H 凝胶的热力学模型 N(C)ASH_ss 并确定了其热力学参数。N(C)ASH_ss 模型包括 8 个凝胶单元(见表 4)，其中前 4 个单元用来描述 N-A-S-H 凝胶，而后 4 个单元是用来考虑溶液环境中 Ca^{2+}对 N-A-S-H 凝胶化学组成的影响，这是因为溶液中 Ca^{2+}会通过离子交换替代 N-A-S-H 凝胶中约 90%的 Na^+，进而影响 N-A-S-H 凝胶的化学组成[35]。基于硅酸盐水泥体系的热力学数据库，通过引入 N(C)ASH_ss 模型及其热力学参数，即可建立碱激发低钙体系的热力学数据库。

表 4 N(C)ASH_ss 模型的分解反应及其溶度积常数(298.15K)[38]

Table 4 Dissociation reactions and solubility products of N(C)ASH_ss (298.15K)[38]

Solids	Molar ratios		Dissociation reactions	$\lg(K_{sp}^{\Theta})$
	Ca/Si	Al/Si		
NASH_1-1[a]	0	1.00	$(Na_2O)_{0.5}\cdot(Al_2O_3)_{0.5}\cdot(SiO_2)_1\cdot(H_2O)_1+2OH^- \leftrightarrow SiO_3^{2-}+AlO_2^-+Na^++2H_2O$	–6.51
NASH_2-1	0	0.50	$(Na_2O)_{0.5}\cdot(Al_2O_3)_{0.5}\cdot(SiO_2)_2\cdot(H_2O)_1+4OH^- \leftrightarrow 2SiO_3^-+AlO_2^-+Na^++3H_2O$	–8.01
NASH_3-1	0	0.33	$(Na_2O)_{0.5}\cdot(Al_2O_3)_{0.5}\cdot(SiO_2)_3\cdot(H_2O)_1+6OH^- \leftrightarrow 3SiO_3^{2-}+AlO_2^-+Na^++4H_2O$	–9.51
NASH_4-1	0	0.25	$(Na_2O)_{0.5}\cdot(Al_2O_3)_{0.5}\cdot(SiO_2)_4\cdot(H_2O)_1+8OH^- \leftrightarrow 4SiO_3^{2-}+AlO_2^-+Na^++5H_2O$	–11.01
NCASH_1-0.1	0.450 0	1.00	$(Na_2O)_{0.05}\cdot(CaO)_{0.45}\cdot(Al_2O_3)_{0.5}\cdot(SiO_2)_1\cdot(H_2O)_1+2OH^- \leftrightarrow SiO_3^{2-}+AlO_2^-+0.45Ca^{2+}+0.1Na^++2H_2O$	–8.51
NCASH_2-0.1	0.225 0	0.50	$(Na_2O)_{0.05}\cdot(CaO)_{0.45}\cdot(Al_2O_3)_{0.5}\cdot(SiO_2)_2\cdot(H_2O)_1+4OH^- \leftrightarrow 2SiO_3^{2-}+AlO_2^-+0.45Ca^{2+}+0.1Na^++3H_2O$	–10.01
NCASH_3-0.1	0.150 0	0.33	$(Na_2O)_{0.05}\cdot(CaO)_{0.45}\cdot(Al_2O_3)_{0.5}\cdot(SiO_2)_3\cdot(H_2O)_1+6OH^- \leftrightarrow 3SiO_3^{2-}+AlO_2^-+0.45Ca^{2+}+0.1Na^++4H_2O$	–11.51
NCASH_4-0.1	0.112 5	0.25	$(Na_2O)_{0.05}\cdot(CaO)_{0.45}\cdot(Al_2O_3)_{0.5}\cdot(SiO_2)_4\cdot(H_2O)_1+8OH^- \leftrightarrow 4SiO_3^{2-}+AlO_2^-+0.45Ca^{2+}+0.1Na^++5H_2O$	–13.01

a. The first and second number after N(C)ASH represent the molar ratio of Si/Al and Na/Al in the solid solution member, respectively.

2.3 碱激发中钙体系的热力学数据库

碱激发中钙体系的反应产物包含碱激发高钙体系和碱激发低钙体系的反应产物。通过联合碱激发高钙体系和碱激发低钙体系的热力学数据库，即可建立碱激发中钙体系的热力学数据库。碱激发中钙体系热力学数据库的准确性和完整性取决于碱激发高钙体系和碱激发低钙体系热力学数据库的质量。

3 碱激发材料的热力学模拟研究

3.1 碱激发材料的热力学模拟方法

在碱激发材料的热力学模拟研究中，一般根据给定的前驱体反应度、反应温度和热力学数据库，假设前驱体活性组分同步溶解，采用热力学计算软件 GEM-Selektor v.3 (GEMS, https://gems.web.psi.ch/) 进行热力学计算。GEMS 软件通过使系统的 Gibbs 自由能最小化来计算给定温度和压强下系统处于平衡状态时各物相的组成，已被广泛用于碱激发材料和普通水泥基材料的热力学模拟研究[32–33, 39–40]。

GEMS 软件采用扩展的 Debye-Hückel 公式[式(1)]来计算离子活度系数[41–42]，其准确计算的溶液离子强度范围约为 1~2 mol/L[43]。由于碱激发剂的引入，碱激发材料孔溶液的离子强度一般约为 1~3 mol/L[15, 44]。目前，基于 GEMS 软件的热力学模拟研究一般认为，尽管碱激发材料孔溶液离子强度略微超出式(1)的准确计算范围，但不会对热力学计算结果造成较大影响[38, 45]。

$$\lg\gamma_j=\frac{-A_\gamma z_j^2\sqrt{I}}{1+\dot{a}B_\gamma\sqrt{I}}+b_\gamma I+lg\frac{x_{jw}}{X_w} \tag{1}$$

式中：γ_j 和 z_j 分别是离子 j 的活度系数和所带电荷；A_γ 和 B_γ 是静电参数；I 是溶液的离子强度；x_{jw} 是水的摩尔数；X_w 是溶液中离子和水的总摩尔数；$\dot{a}$ 和 b_γ 分别是平均离子尺寸和带电离子相互作用参数。

3.2　碱激发高钙体系的热力学模拟研究

基于硅酸盐水泥水化产物 C-S-H 凝胶的热力学模型和热力学参数，Lothenbach 等[44]对碱激发矿渣水泥物相演变进行了热力学模拟研究，并通过设置凝胶中 Al/Si 比值和凝胶中 Na 与溶液中 Na 的比值来考虑碱激发矿渣水化产物 C-(N-)A-S-H 凝胶中 Al 和 Na 的含量，研究发现碱激发剂组成主要影响 C-S-H 凝胶中的 Ca/Si 比和孔溶液化学组成，对反应产物类型没有影响。随后，Haha 等[46–47]采用类似方法模拟研究了矿渣化学组成对碱激发矿渣水泥反应产物组成的影响，结果表明矿渣中 MgO 含量升高会增加含氢氧根水滑石的生成量，而矿渣中 Al_2O_3 含量升高会增加水化钙铝黄长石的生成量。尽管基于 C-S-H 凝胶的热力学模拟能够较好预测碱激发矿渣水泥的物相组成，但未从根本上提出描述 C-(N-)A-S-H 凝胶的热力学模型，导致热力学模拟仍需通过试验测试来校正 C-(N-)A-S-H 凝胶中 Al 和 Na 的含量。

Myers 等[32]基于 C-S-H 凝胶的结构模型，考虑 Al 和 Na 对凝胶结构和组成的影响，从根本上提出描述 C-(N-)A-S-H 凝胶的热力学模型 CNASH_ss 并确定了其热力学参数，由此建立和完善了碱激发高钙体系的热力学数据库。随后，关于碱激发高钙体系的热力学模拟研究逐渐增多，并取得了丰硕研究成果。Myers 等[17, 32–33]基于已建立的碱激发高钙体系热力学数据库，针对不同碱激发剂和不同矿渣化学组成，展开了一系列的热力学模拟研究。结果表明，热力学模拟不仅可以预测碱激发矿渣水泥物相的演变，而且可以计算不同矿渣化学组成下碱激发矿渣水泥反应产物的物相组成图(见图 3)，进而为碱激发矿渣水泥化学性能的精细化设计提供理论依据。

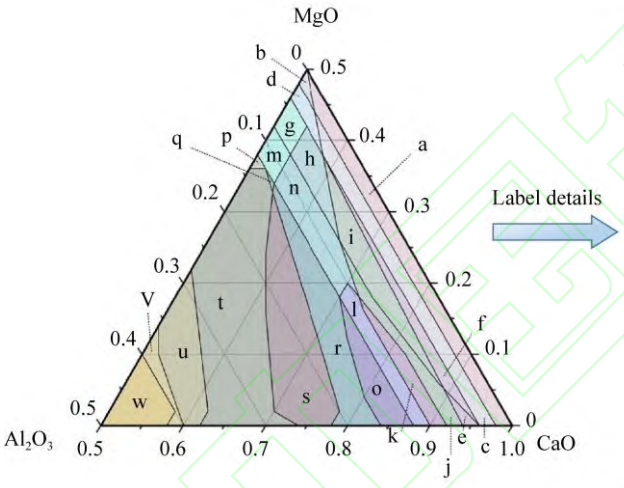

Region	Simulated solid phase assemblage										
	1	2	3	4	5	6	7	8	9	10	11
a	X	-	-	-	-	-	-	-	MT	MT	-
b	X	-	-	-	-	-	-	-	-	M	-
c	X	-	-	-	T	-	-	-	MT	MT	-
d	X	-	-	-	T	-	-	-	-	M	-
e	X	-	-	-	T	M	-	-	M	-	-
f	X	-	-	-	T	M	-	-	MT	MT	-
g	X	MT	-	-	MT	-	-	-	-	MT	-
h	X	MT	-	-	MT	MT	-	-	-	MT	-
i	X	MT	-	-	T	-	-	-	MT	MT	-
j		MT	-	-	T	M	-	-	MT	-	-
k	X	MT	-	MT	T	M	-	-	T	-	-
l	X	MT	-	MT	T	M	-	-	-	-	-
m	X	M	-	-	M	-	-	-	-	-	-
n	X	M	-	-	MT	MT	-	-	-	-	-
o	X	MT	MT	MT	T	M	-	-	-	-	-
p	X	M	-	-	M	-	T	-	-	-	-
q	X	M	T	-	M	-	-	-	-	-	-
r	X	MT	XMT	-	MT	MT	-	-	-	-	-
s	XM	MT	XMT	-	MT	MT	MT	-	-	-	-
t	XM	MT	XMT	-	MT	-	MT	-	-	-	-
u	MT	MT	XMT	-	M	-	M	T	-	-	-
v	-	MT	X	-	M	-	M	MT	-	-	-
w	-	MT	X	-	M	-	M	MT	-	-	MT

Simulated solid reaction products are: 1, CNASH_ss; 2, MA-OH-LDH_ss; 3, strätlingite; 4, katoite; 5, ettringite; 6, $C_4A\bar{S}Hss$; 7, natrolite; 8, Ca-heulandite; 9, portlandite; 10, brucite; 11, $AH_{3(mc)}$. X, M and T represent major, minor and trace amounts, respectively. Multiple letters are used where more than one category applies.

图 3　碱激发矿渣水泥反应产物相图[17]

Fig. 3　Phase diagram of alkali-activated slag cement[17]

此外，Ye 等[48]采用热力学模拟计算碱激发矿渣水泥在不同反应度下的物相组成，根据物相组成计算反应后的总体积(V_t)，并结合碱激发矿渣水泥初始总体积(V_0)，计算碱激发矿渣水泥反应后的化学收缩(V_0–V_t)，结果表明化学收缩的热力学计算结果与试验结果相比，其误差为 4.81%~19.22%。为了克服传统以反应度为维度表征的热力学模拟结果无法直接与以时间为维度表征的试验测试结果进行对比分析，Zuo 等[49]通过引入反应动力学控制方程，结合选择性溶解法和水化热估算法确定矿渣反应度，进而建立矿渣反应度与时间的映射关系函数[Eq. (2)]，然后在不同时间所对应的矿渣反应度下进行热力学模拟，从而实现碱激发矿渣水泥物相演变在时间维度上的热力学模拟研究。通过对比和分析孔溶液化学组成、化学结合水、反应产物量和反应产物化学组成的热力学计算结果和试验结果，研究者认为热力学模拟能够预测和研究碱激发矿渣水泥物化性质随时间的变化规律[49]。然而，水化热估算法确定的矿渣反应度偏高，如何在时间维度上连续且准确确定矿渣反应度仍需进一步研究。

$$\ln\left[1-\frac{2}{3}\alpha(t)-\left(1-\alpha(t)\right)^{2/3}\right]=\frac{1}{N}\ln k+\frac{1}{N}\ln t \quad (2)$$

式中：$\alpha(t)$ 为矿渣反应度；k 为速率常数；N 为反应级数；t 为时间。

碱激发材料在侵蚀性介质作用下的物相变化是表征其耐久性能的重要方面。近些年来，学者们开始通过热力学模拟侵蚀性介质作用下的物相演变来研究碱激发高钙体系的耐久性能，并取得了一定研究成果。具体表现为以下 2 个方面：

1) 基于热力学模拟研究单一因素作用下碱激发矿渣水泥的耐久性能

基于碱激发高钙体系热力学数据库，Ke 等[50]引入含碳酸根水滑石相和其他碳化产物相，采用热力学模拟研究了碳化作用下碱激发矿渣水泥的物相演变过程(见图 4)，指出矿渣组成主要影响碳化过程中晶体产物的化学性能，而碱激发剂组成主要影响碳化后的物相演变过程和孔溶液 pH 值，例如在相同碳化程度下碳酸钠激发矿渣水泥比硅酸钠激发矿渣水泥具有更高的孔溶液 pH 值。通过引入含氯离子水滑石的热力学模型和热力学参数，Zuo 等[51]对氯盐侵蚀下的碱激发矿渣水泥相演变过程进行了热力学模拟研究，发现氯盐中阳离子类型和矿渣化学组成对碱激发矿渣水泥物相演变、孔溶液组成和氯离子化学结合都有重要影响，而且 C-(N-)A-S-H 凝胶在氯盐侵蚀下发生了脱钙、脱铝现象，导致其平均链长发生变化。此外，研究者通过引入含硫酸根水滑石的热力学模型和热力学参数，进一步对硫酸盐侵蚀下碱激发矿渣水泥的相演变过程展开了热力学模拟研究，总结了硫酸钠和硫酸镁侵蚀的差异(见表 5)，结果表明在孔溶液 pH 值变化、C-(N-)A-S-H 凝胶腐蚀(脱钙、脱铝)和产物膨胀方面，硫酸镁侵蚀比硫酸钠侵蚀更严重，分析认为相比于硫酸钠侵蚀，硫酸镁侵蚀过程中镁离子也参与了反应，形成水镁石和含氢氧根水滑石，消耗孔溶液中氢氧根离子，导致孔溶液 pH 值下降，而孔溶液碱性环境变弱致使 C-(N-)A-S-H 凝胶不稳定，易于脱钙、脱铝，游离出来的钙和铝促进膨胀性产物钙矾石和石膏的生成，最终导致碱激发矿渣水泥产物膨胀显著[52]。

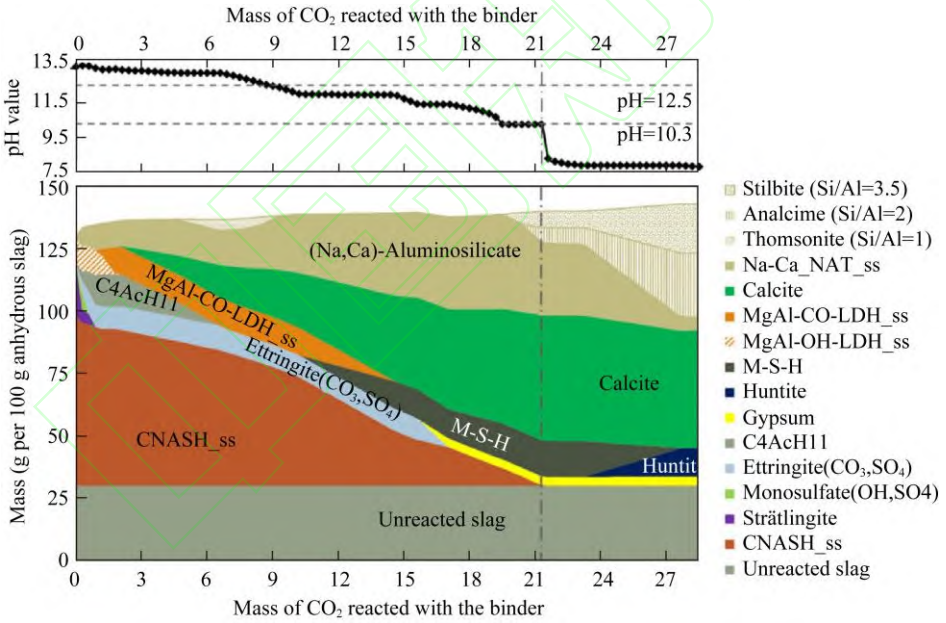

water/solid=0.4, Na_2O/slag ratio=4%, Na_2O/SiO_2 ratio=1, reaction degree of slag=70%, and concentration of CO_2=1%.

图 4 热力学模拟加速碳化下碱激发矿渣水泥的物相演变和孔溶液 pH 值变化[50]

Fig. 4 Thermodynamic modelling of the phase evolution and pore solution pH value of alkali-activated slag cement under stepwise accelerated carbonation[50]

2) 基于热力学模拟研究多因素耦合作用下碱激发矿渣水泥的耐久性能

针对氯盐和硫酸盐耦合侵蚀下碱激发矿渣水泥的耐久性能，Zuo 等[53]通过热力学模拟研究首次指出：氯盐和硫酸盐耦合侵蚀不仅具有单一硫酸盐和单一氯盐侵蚀的特点，还显示出明显的耦合效应，促使含氯离子水滑石的生成，抑制 Friedel 盐和水化硅酸镁的生成，降低化学结合氯离子量。此外，Reddy 等[54]通过热力学模拟研究了碱激发矿渣水泥在海水侵蚀下反应产物的稳定性，发现主要反应产物 C-(N-)A-S-H 凝胶和含氢氧根水滑石在较少海水侵蚀时比较稳定，而在侵蚀的海水量增加时分解为

表 5　硫酸钠和硫酸镁侵蚀碱激发矿渣水泥的差异[52]

Table 5　Differences induced by sodium sulfate attack and magnesium sulfate attack on alkali-activated slag[52]

Items	Sodium sulfate attack	Magnesium sulfate attack
Change of pH in pore solution	Increases with the maximums of 0.21 (NH) and 0.41 (NS)	Decreases with maximums of 2.06 (NH) and 1.72 (NS)
Reduction of Ca/Si in C-(N-)A-S-H gel	Maximum reductions of 0.11 (NH) and 0.16 (NS)	Maximum reductions of 0.28 (NH) and 0.30 (NS)
Reduction of Al/Si in C-(N-)A-S-H gel	Maximum reductions of 0.02 (NH) and 0.03 (NS)	Maximum reductions of 0.11 (NH) and 0.10 (NS)
Solid phase expansion (γ, %)	Maximum values of 4.79 (NH) and 8.96 (NS)	Increases up to 43.50 (NH) and 38.41 (NS)

NH and NS represent sodium hydroxide activated slag cement and sodium silicate activated slag cement, respectively.

钙矾石和水化硅酸镁，同时碱激发矿渣水泥的体积显著增加。

3.3　碱激发低钙体系的热力学模拟

相较于碱激发高钙体系，碱激发低钙体系的热力学模拟研究仍比较匮乏。基于建立的低钙体系热力学数据库和反应动力学控制方程，Zuo[38]首次采用热力学模拟对碱激发粉煤灰物相组成在时间维度上的演变过程展开了研究(见图 5a)，发现增加碱当量(Na_2O/粉煤灰)会导致碱激发粉煤灰中 N-(C-)A-S-H 凝胶含量降低和钠沸石含量增加，而增加激发剂模数(SiO_2/Na_2O)会使 N-(C-)A-S-H 凝胶含量增加和钠沸石含量降低。此外，热力学模拟结果还显示碱激发粉煤灰在反应过程中并没有明显的化学收缩，分析认为可能存在两个方面的原因：一是 N-(C-)A-S-H 凝胶比 C-(N-)A-S-H 凝胶具有更低的化学结合水(分别为 5.29%~11.44%和 12.56%~23.81%)，产生的化学收缩较小；二是生成的钠沸石的密度较低(2.375 g/cm^3)[55]，具有一定膨胀性，可以弥补潜在的化学收缩。图 5b 展示了碱激发粉煤灰孔溶液化学组成的热力学模拟结果与试验测试结果[38]，尽管孔溶液中 Si、Na、Ca 元素和 OH^- 离子浓度的热力学模拟结果的误差在±1 个数量级之内，与试验测试误差相近[32]，但 Al 元素浓度的热力学模拟结果与试验结果相差几个数量级，这说明描述 N-A-S-H 凝胶的热力学模型及其热力学参数仍需要更多的试验数据进行校正。

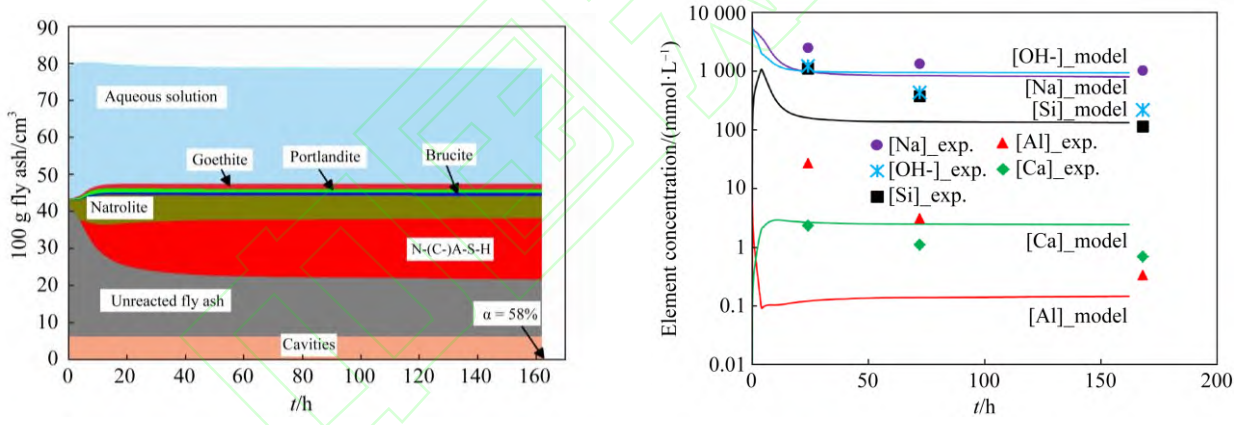

(a) Phase evolution　　(b) Pore solution composition

图 5　热力学模拟氢氧化钠激发粉煤灰的物相演变过程和孔溶液中元素/离子浓度(水胶比为 0.35，碱当量为 6.2%，反应温度为 60 ℃)[38]

Fig. 5　Thermodynamic modelling of the phase evolution and pore solution composition of sodium hydroxide activated fly ash (in the calculations, water/fly ash ratio= 0.35, Na_2O/slag ratio= 6.2%, reaction temperature=60 ℃)[38]

3.4　碱激发中钙体系的热力学模拟研究

由于碱激发中钙体系的热力学数据库仍不完善，相关热力学模拟研究较少。当矿渣和粉煤灰以质量比 1:1 复合，其碱激发复合胶凝材料物相演变的热力学模拟结果如图 6a 所示，结果表明[38]：碱激发矿渣-粉煤灰复合胶凝材料中 C-(N-)A-S-H 凝胶和 N-A-S-H 凝胶同时存在，且 C-(N-)A-S-H 凝胶对总体积增长的贡献大于 N-A-S-H 凝胶；此外，碱激发矿渣-粉煤灰复合胶凝材料的化学收缩介于碱激发矿渣和碱激发粉煤灰的化学收缩之间，且在反应早期出现了微膨胀，分析认为这是由生成的钠沸石所致，而随着反应的进行，钠沸石开始分解，导致微膨胀消失，化学收缩开始展现。最近，Chen 等[56]利用热力学模拟研究了不同碱当量条件下碱激发 MSWI 底灰的物相变化(见图 6b)，主要反应产物为 C-(N-)A-S-H 凝胶、N-A-S-H 凝胶和沸石。在碱当

量为 10%时，C-(N-)A-S-H 凝胶含量与 N-A-S-H 凝胶和沸石含量之和的比值为 0.95，略低于试验值 1.26[29, 57]，这主要是由于相同碱当量下所采用碱激发剂的类型不同所致(前者为氢氧化钠，后者为硅酸钠)。随着碱当量增加，C-(N-)A-S-H 凝胶含量基本保持不变，而在碱当量高于 4.5%时，N-A-S-H 凝胶含量开始降低，钠沸石含量逐渐增加。

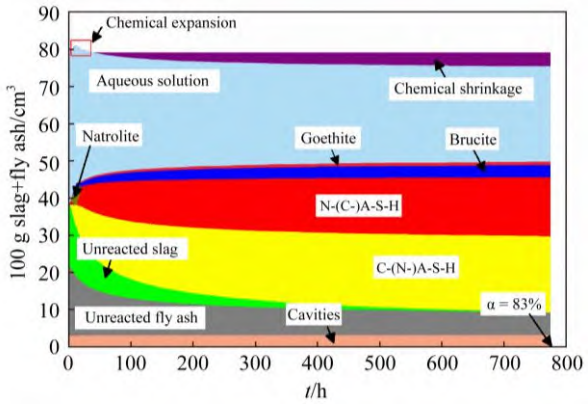

(a) Alkali-activated slag and fly ash (slag/fly ash=1:1, water/binder ratio=0.4, Na_2O/binder ratio= 6%, and activator modulus=0.93)

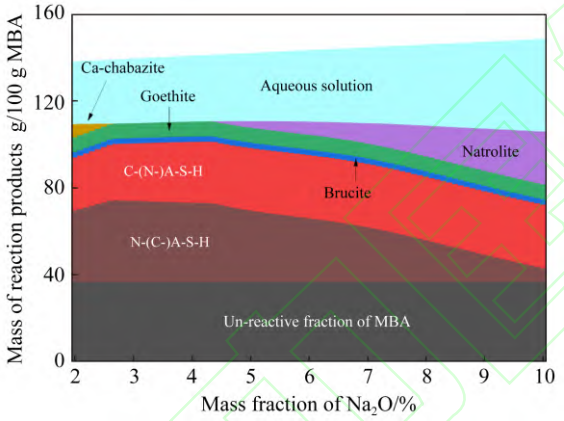

(b) Alkali-activated MSWI bottom ash (water/bottom ash ratio=0.35, activator is NaOH)

图 6　热力学模拟碱激发矿渣-粉煤灰复合胶凝材料和碱激发 MSWI 底灰的物相演变过程[38, 56]

Fig. 6　Thermodynamic modelling of the phase evolution of alkali-activated slag and fly ash, and alkali-activated MSWI bottom ash[38, 56]

4　基于热力学模拟耦合其他模拟技术的碱激发材料数值研究

热力学模拟在处理复杂化学反应和预测反应产物及溶液化学组成方面具有很好的鲁棒性。因此，热力学模拟除了单独用于研究材料中化学反应引起的物相变化之外，还可与其他模拟技术耦合对材料性能展开数值研究。热力学模拟与其他模拟技术相结合的数值研究方法已广泛应用于普通硅酸盐水泥体系[58–60]。然而相比于普通硅酸盐水泥体系，碱激发材料由于发展历程较短，其基于热力学模拟耦合其他模拟技术的数值研究才刚起步。

Mundra 等[22]基于 Fick 第二定律和热力学模拟，建立了碱激发矿渣混凝土中氯离子传输模型，该模型首次通过热力学模拟将碱激发矿渣水泥原材料组成、反应产物组成与传输过程中的氯离子固化效应联系起来，避免采用经验公式考虑氯离子固化效应，因此极大提升了数值模拟和预测氯离子传输的准确性。针对原材料组成多样性所带来的碱激发材料设计困难，Ke 等[61]基于热力学模拟，以数据驱动的方式，建立了碱激发材料组成与强度相互关联的机器学习模型，尽管前驱体来源多样，但原材料组成、反应产物组成与碱激发材料性能之间仍存在内在联系，基于热力学模拟和数据驱动的机器学习模型将为基于性能的碱激发材料设计提供新途径。Zuo 等[62]结合格子 Boltzmann 方法和热力学模拟技术，首次建立了模拟碱激发矿渣水泥浆微结构形成的数值模型 GeoMicro3D (见图 7a)，并对碱激发矿渣水泥反应

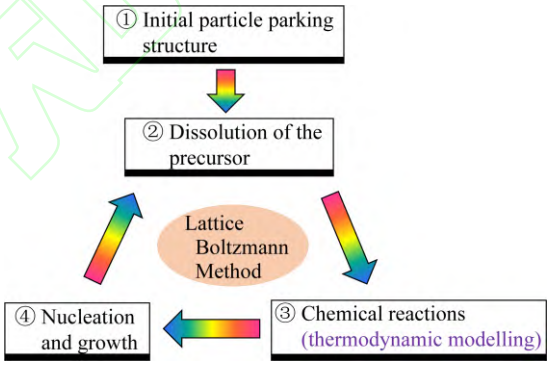

(a) GeoMicro3D structure

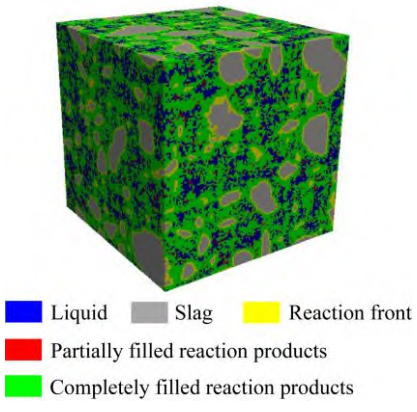

(b) Simulated microstructure

图 7　GeoMicro3D 模型结构示意图和模拟碱激发矿渣水泥浆 7 d 的微观结构[62]

Fig. 7　Schematic illustration of the structure of GeoMicro3D model and the simulated microstructure of alkali-activated slag paste at 7 d[62]

过程和微结构演变进行了数值模拟研究(见图 7b)，不仅揭示了化学反应、多离子传输和微结构形成之间的交互作用机制，而且为研究碱激发矿渣水泥反应过程和微观结构形成提供了先进的数值模拟方法，拓展了碱激发矿渣水泥体系的研究手段。

5　结论与展望

热力学模拟在研究碱激发材料化学反应引起的物相演变和耐久性能等方面展现出强大优势。首先，热力学模拟能够预测碱激发材料反应产物和孔溶液的组成，有助于研究碱激发材料反应机理以及各种因素的影响机制。其次，热力学模拟能够计算侵蚀性介质作用下碱激发材料的物相演变过程，进而研究碱激发材料的破坏机理及其微观作用机制。最后，热力学模拟还可与其他数值模拟手段结合，研究碱激发材料的微结构形成、耐久性能以及实现基于性能的碱激发材料组成设计。目前，尽管热力学模拟研究已经取得一定成果，但仍存在一些问题需要继续深入研究：

1) 碱激发低钙体系的热力学数据库不健全是导致碱激发低、中钙体系的热力学模拟研究发展迟缓的重要原因。尽管已有学者提出描述 N-A-S-H 凝胶的热力学模型 N(C)ASH_ss，进而建立了碱激发低钙体系的热力学数据库，但 N(C)ASH_ss 是基于半理论-半试验的经验模型，其准确性仍需要更多的试验数据进行校正。随着原子、分子尺度模拟技术的发展，有望通过第一性原理计算和分子动力学模拟提出描述 N-A-S-H 凝胶的热力学模型并确定其热力学参数。

2) 由于碱激发剂的引入，碱激发材料孔溶液含有丰富的离子，导致其离子强度可能超出扩展的 Debye-Hückel 公式的准确计算范围，进而影响热力学计算结果的准确性。这种影响有多大、是否可以忽略等问题需要进一步研究。此外，为了能够使用 Pitzer 模型计算离子活度系数，有必要改进 GEMS 应用程序。

3) 在热力学模拟研究中，一般假设前驱体活性组分同步溶解，然而碱激发材料实际反应过程中，由于前驱体结构和组成分布不均匀，活性组分并不是同步溶解。因此，前驱体活性组分溶解的非均匀性是热力学模拟研究需要进一步考虑的问题。

4) 碱激发材料物相演变实际上是热力学和动力学相互耦合下的变化过程，然而大多热力学模拟研究通常只关注平衡状态时的物相组成，缺乏考虑达到平衡状态过程中的动力学问题和反应的中间产物，导致研究结论和提出的模型仍具有一定局限性。如何在热力学模拟研究中同时考虑溶解速率和反应速率等动力学参数以及反应中间产物，是当前和未来热力学模拟研究的重点。

5) 物相演变、微结构损伤和介质传输是研究碱激发材料耐久性能的重要方面，然而目前基于热力学模拟的碱激发材料耐久性研究主要关注侵蚀介质化学作用下的物相演变，缺乏考虑物相演变与微结构损伤、介质传输的交互作用。在今后的数值研究中，有必要考虑物相-结构-传输的交互作用，建立侵蚀介质作用下的化学-损伤-传输模型，进而开展碱激发材料耐久性能的数值模拟研究。

参考文献:

[1] DUXSON P, FERNÁNDEZ-JIMÉNEZ A, PROVIS J L, et al. Geopolymer technology: The current state of the art[J]. J Mater Sci, 2007, 42(9): 2917–2933.

[2] 阎培渝. 碱激发胶凝材料发展瓶颈在哪里[J]. 硅酸盐学报, 2022, 50(8): 2067–2069.
YAN Peiyu. J Chin Ceram Soc, 2022, 50(8): 2067–2069.

[3] SHI C J, QU B, PROVIS J L. Recent progress in low-carbon binders[J]. Cem Concr Res, 2019, 122: 227–250.

[4] NEHDI M L, YASSINE A. Mitigating Portland cement CO2 emissions using alkali-activated materials: System dynamics model[J]. Materials, 2020, 13(20): 4685.

[5] DEVENTER J S J, WHITE C E, MYERS R J. A roadmap for production of cement and concrete with low-CO2 emissions[J]. Waste Biomass Valorization, 2021, 12(9): 4745–4775.

[6] 王爱国, 郑毅, 张祖华, 等. 碱激发材料与普通硅酸盐水泥和混凝土的耐久性能比较[J]. 工程, 2020, 6(6): 237–261.
WANG Aiguo, ZHENG Yi, ZHANG Zuhua, et al. Eng, 2020, 6(6): 237–261.

[7] JIANG D D, SHI C J, ZHANG Z H. Recent progress in understanding setting and hardening of alkali-activated slag (AAS) materials[J]. Cem Concr Compos, 2022, 134: 104795.

[8] PROVIS J L, BERNAL S A. Geopolymers and related alkali-activated materials[J]. Annu Rev Mater Res, 2014, 44: 299–327.

[9] VAN DEVENTER J S J, PROVIS J L, DUXSON P. Technical and commercial progress in the adoption of geopolymer cement[J]. Miner Eng, 2012, 29: 89–104.

[10] GIERGICZNY Z. Fly ash and slag[J]. Cem Concr Res, 2019, 124: 105826.

[11] LI C, SUN H H, LI L T. A review: The comparison between alkali-activated slag (Si+Ca) and metakaolin (Si+Al) cements[J]. Cem Concr Res, 2010, 40(9): 1341–1349.

[12] PROVIS J L, LUKEY G C, VAN DEVENTER J S J. Do geopolymers actually contain nanocrystalline zeolites? A reexamination of existing results[J]. Chem Mater, 2005, 17(12): 3075–3085.

[13] ROWLES M R, O'CONNOR B H. Chemical and structural microanalysis of aluminosilicate geopolymers synthesized by sodium silicate activation of metakaolinite[J]. J Am Ceram Soc, 2009, 92(10): 2354–2361.

[14] DAI X D, AYDIN S, YARDIMCI M Y, et al. Early age reaction, rheological properties and pore solution chemistry of NaOH-activated slag mixtures[J]. Cem Concr Compos, 2022, 133: 104715.

[15] ZUO Y B, NEDELJKOVIĆ M, YE G. Pore solution composition of alkali-activated slag/fly ash pastes[J]. Cem Concr Res, 2019, 115: 230–250.

[16] PUERTAS F, FERNÁNDEZ-JIMÉNEZ A, BLANCO-VARELA M T. Pore solution in alkali-activated slag cement pastes. Relation to the composition and structure of calcium silicate hydrate[J]. Cem Concr Res, 2004, 34(1): 139–148.

[17] MYERS R J, BERNAL S A, PROVIS J L. Phase diagrams for alkali-activated slag binders[J]. Cem Concr Res, 2017, 95: 30–38.

[18] BEN HAHA M, LE SAOUT G, WINNEFELD F, et al. Influence of activator type on hydration kinetics, hydrate assemblage and microstructural development of alkali activated blast-furnace slags[J]. Cem Concr Res, 2011, 41(3): 301–310.

[19] MA Y, HU J, YE G. The effect of activating solution on the mechanical strength, reaction rate, mineralogy, and microstructure of alkali-activated fly ash[J]. J Mater Sci, 2012, 47(11): 4568–4578.

[20] ZHANG Z M, CHEN R, HU J, et al. Corrosion behavior of the reinforcement in chloride-contaminated alkali-activated fly ash pore solution[J]. Compos B Eng, 2021, 224: 109215.

[21] ÖZÇELIK V O, WHITE C E. Nanoscale charge-balancing mechanism in alkali-substituted calcium–silicate–hydrate gels[J]. J Phys Chem Lett, 2016, 7(24): 5266–5272.

[22] MUNDRA S, PRENTICE D P, BERNAL S A, et al. Modelling chloride transport in alkali-activated slags[J]. Cem Concr Res, 2020, 130: 106011.

[23] LIU Q F, CAI Y X, PENG H, et al. A numerical study on chloride transport in alkali-activated fly ash/slag concretes[J]. Cem Concr Res, 2023, 166: 107094.

[24] ZUO Y B, YE G. Lattice Boltzmann simulation of the dissolution of slag in alkaline solution using real-shape particles[J]. Cem Concr Res, 2021, 140: 106313.

[25] PACHECO-TORGAL F, LABRINCHA J, LEONELLI C, et al, Handbook of alkali-activated cements, mortars and concretes [M], Elsevier, 2014.

[26] ISMAIL I, BERNAL S A, PROVIS J L, et al. Modification of phase evolution in alkali-activated blast furnace slag by the incorporation of fly ash[J]. Cem Concr Compos, 2014, 45: 125–135.

[27] PULIGILLA S, MONDAL P. Co-existence of aluminosilicate and calcium silicate gel characterized through selective dissolution and FTIR spectral subtraction[J]. Cem Concr Res, 2015, 70: 39–49.

[28] BERNAL S A, PROVIS J L, WALKLEY B, et al. Gel nanostructure in alkali-activated binders based on slag and fly ash, and effects of accelerated carbonation[J]. Cem Concr Res, 2013, 53: 127–144.

[29] MALDONADO-ALAMEDA À, GIRO-PALOMA J, ALFOCEA-ROIG A, et al. Municipal solid waste incineration bottom ash as sole precursor in the alkali-activated binder formulation[J]. Appl Sci, 2020, 10(12): 4129.

[30] ZHU W P, CHEN X, STRUBLE L J, et al. Quantitative characterization of aluminosilicate gels in alkali-activated incineration bottom ash through sequential chemical extractions and deconvoluted nuclear magnetic resonance spectra[J]. Cem Concr Compos, 2019, 99: 175–180.

[31] MYERS R J, BERNAL S A, SAN NICOLAS R, et al. Generalized structural description of calcium–sodium aluminosilicate hydrate gels: the cross-linked substituted tobermorite model[J]. Langmuir, 2013, 29(17): 5294–5306.

[32] MYERS R J, BERNAL S A, PROVIS J L. A thermodynamic model for C-(N-) A-S-H gel: CNASH_ss. Derivation and validation[J]. Cem Concr Res, 2014, 66: 27–47.

[33] MYERS R J, LOTHENBACH B, BERNAL S A, et al. Thermodynamic modelling of alkali-activated slag cements[J]. Appl Geochem, 2015, 61: 233–247.

[34] LOTHENBACH B, KULIK D A, MATSCHEI T, et al. Cemdata18: A chemical thermodynamic database for hydrated Portland cements and alkali-activated materials[J]. Cem Concr Res, 2019, 115: 472–506.

[35] GARCÍA-LODEIRO I, FERNÁNDEZ-JIMÉNEZ A, PALOMO A, et al. Effect of calcium additions on N-A-S-H cementitious gels[J]. J Am Ceram Soc, 2010, 93(7): 1934–1940.

[36] BELL J L, SARIN P, DRIEMEYER P E, et al. X-Ray pair distribution function analysis of a metakaolin-based, $KAlSi_2O_6$ $5.5H_2O$ inorganic polymer (geopolymer)[J]. J Mater Chem, 2008, 18(48): 5974–5981.

[37] WHITE C E, PROVIS J L, PROFFEN T, et al. The effects of temperature on the local structure of metakaolin-based geopolymer binder: A neutron pair distribution function investigation[J]. J Am Ceram Soc, 2010, 93(10): 3486–3492.

[38] ZUO Y, Experimental study and numerical simulation of the reaction process and microstructure formation of alkali-activated materials[D]. Delft University of Technology, 2019.

[39] BALONIS M. Thermodynamic modelling of temperature effects on the mineralogy of Portland cement systems containing chloride[J]. Cem Concr Res, 2019, 120: 66–76.

[40] CAO Y Z, GUO L P, CHEN B, et al. Thermodynamic modelling and experimental investigation on chloride binding in cement exposed to chloride and chloride-sulfate solution[J]. Constr Build Mater, 2020, 246: 118398.

[41] KULIK D A, WAGNER T, DMYTRIEVA S V, et al. GEM-Selektor geochemical modeling package: Revised algorithm and GEMS3K numerical kernel for coupled simulation codes[J]. Comput Geosci, 2013, 17(1): 1–24.

[42] WAGNER T, KULIK D A, HINGERL F F, et al. Gem-selektor geochemical modeling package: Tsolmod library and data interface for multicomponent phase models[J]. Can Mineral, 2012, 50(5): 1173–1195.

[43] HELGESON H C, KIRKHAM D H, FLOWERS G C. Theoretical prediction of the thermodynamic behavior of aqueous electrolytes by high pressures and temperatures; IV, Calculation of activity coefficients, osmotic coefficients, and apparent molal and standard and relative partial molal properties to 600 degrees C and 5kb[J]. Am J Sci, 1981, 281(10): 1249–1516.

[44] LOTHENBACH B, GRUSKOVNJAK A. Hydration of alkali-activated slag: Thermodynamic modelling[J]. Adv Cem Res, 2007, 19(2): 81–92.

[45] MYERS R J. Thermodynamic Modelling of CaO-Al_2O_3-SiO_2-H_2O-Based Cements[D]. University of Sheffield, 2015.

[46] BEN HAHA M, LOTHENBACH B, LE SAOUT G, et al. Influence of slag chemistry on the hydration of alkali-activated blast-furnace slag—part I: Effect of MgO[J]. Cem Concr Res, 2011, 41(9): 955–963.

[47] BEN HAHA M, LOTHENBACH B, LE SAOUT G, et al. Influence of slag chemistry on the hydration of alkali-activated blast-furnace slag—part II: Effect of Al_2O_3[J]. Cem Concr Res, 2012, 42(1): 74–83.

[48] YE H L, RADLIŃSKA A. Quantitative analysis of phase assemblage and chemical shrinkage of alkali-activated slag[J]. J Adv Concr

Technol, 2016, 14(5): 245–260.
[49] ZUO Y B, NEDELJKOVIĆ M, YE G. Coupled thermodynamic modelling and experimental study of sodium hydroxide activated slag[J]. Constr Build Mater, 2018, 188: 262–279.
[50] KE X Y, BERNAL S A, PROVIS J L, et al. Thermodynamic modelling of phase evolution in alkali-activated slag cements exposed to carbon dioxide[J]. Cem Concr Res, 2020, 136: 106158.
[51] ZUO Y B. Effect of chloride salt on the phase evolution in alkali-activated slag cements through thermodynamic modelling[J]. Appl Geochem, 2022, 136: 105169.
[52] ZUO Y B. Thermodynamic modeling of the phase evolution in alkali-activated slag cements with sulfate salt exposure[J]. J Am Ceram Soc, 2022, 105(12): 7658–7675.
[53] 左义兵, 廖宜顺, 叶光. 盐耦合侵蚀下碱矿渣水泥相演变的热力学模拟[J]. 建筑材料学报, 2023, 26(1): 7–13.
ZUO Yibing, LIAO Yishun, YE Guang. J Build Mater, 2023, 26(1): 7–13.
[54] REDDY K C, KIM G M, PARK S. Modeling the phase evolution in alkali-activated slag cements upon interaction with seawater[J]. Case Stud Constr Mater, 2022, 17: e01476.
[55] LOTHENBACH B, BERNARD E, MÄDER U. Zeolite formation in the presence of cement hydrates and albite[J]. Phys Chem Earth Parts A/B/C, 2017, 99: 77–94.
[56] CHEN B, ZUO Y, ZHANG S, et al. Reactivity and leaching potential of municipal solid waste incineration (MSWI) bottom ash as supplementary cementitious material and precursor for alkali-activated materials[J]. Constr Build Mater, 2023, under review.
[57] MALDONADO-ALAMEDA A, GIRO-PALOMA J, SVOBODOVA-SEDLACKOVA A, et al. Municipal solid waste incineration bottom ash as alkali-activated cement precursor depending on particle size[J]. J Clean Prod, 2020, 242: 118443.
[58] HOSOKAWA Y, YAMADA K, JOHANNESSON B, et al. Development of a multi-species mass transport model for concrete with account to thermodynamic phase equilibriums[J]. Mater Struct, 2011, 44(9): 1577–1592.
[59] GUO B B, HONG Y, QIAO G F, et al. A COMSOL-PHREEQC interface for modeling the multi-species transport of saturated cement-based materials[J]. Constr Build Mater, 2018, 187: 839–853.
[60] SHARMILAN S, STANG H, MICHEL A. A multi-species reactive transport model based on ion-solid phase interaction for saturated cement-based materials[J]. Cem Concr Res, 2022, 159: 106861.
[61] KE X Y, DUAN Y. Coupling machine learning with thermodynamic modelling to develop a composition-property model for alkali-activated materials[J]. Compos B Eng, 2021, 216: 108801.
[62] ZUO Y B, YE G. GeoMicro3D: A novel numerical model for simulating the reaction process and microstructure formation of alkali-activated slag[J]. Cem Concr Res, 2021, 141: 106328.

Phase Evolution and Durability of Alkali-Activated Materials: A Thermodynamic Modelling Review

ZUO Yibing[1,2], *LIAO Yishun*[3], *YANG Yingzi*[4], *YE Guang*[5]
(1. School of Civil and Hydraulic Engineering, Huazhong University of Science and Technology, Wuhan 430074, China; 2. State Environmental Protection Key Laboratory of Mineral Metallurgical Resources Utilization and Pollution Control, Wuhan 430081, China; 3. School of Urban Construction, Wuhan University of Science and Technology, Wuhan 430065, China; 4. Civil Engineering College, Harbin Institute of Technology, Harbin 150090, China; 5. Faculty of Civil Engineering and Geosciences, Delft University of Technology, Delft 2628 CN, Netherlands)

Extended Abstract

Alkali-activated materials (AAMs) are a new class of green cementitious materials in the building materials industry and beneficial to the goals of carbon peaking and carbon neutrality. In comparison with ordinary Portland cement (PC) based materials, however, the raw material composition, reaction products and pore solution composition of AAMs are more complex and thus their reaction mechanisms and performance evolutions still need to be further clarified. Thermodynamic modelling is an effective method in studying AAMs. It can predict the phase assemblage and pore solution composition based on the raw material composition and given reaction conditions, which is of great significance to profoundly investigate and reveal the reaction mechanisms and performance evolutions of AAMs. Currently, thermodynamic modelling has been increasingly applied in AAMs and fruitful results have been achieved. However, a comprehensive review is lacking on the state-of-art in thermodynamic modelling of AAMs. A clear and systematic knowledeg of the principles, thermodynamic databases, methods, challenges and gaps remains inplicit for thermodynamic modelling of AAMs. In this context, the present paper aimed to review and summarize the recent progresses in thermodynamic modelling of AAMs, point out the deficiency gaps of current thermodynamic modelling researches and put forward the relevant perspectives. With this review paper, it is expected to provide theoretical guidance for thermodynamic modelling of AAMs.

Chemical reactions in AAMs follow the laws of thermodynamics. There exists two thermodyanmic equilibriums in AAMs: one is between the precursor and aqueous solution and the other is between the reaction products and aqueous solution. By assuming the thermodynamic equilobriumes, thermmodynamic modelling can be performed to predict the phase assemblage and pore solution composition of AAMs as illustrated in Fig. 2. The accuracy and reliability of thermodynamic modelling results largely denpends on the quality of thermodyanmic database that consits of solubility products (K_{sp}), heat capacity (C_n^{Θ}), entropy (S^{Θ}), Gibbs free energy($\Delta_f G_m^{\Theta}$), enthalpy ($\Delta_f H^{\Theta}$) and molar volume (V^{Θ}) for all solid, liquid and gas phases involved in the system. The

thermodynamicdatabase of AAMs is usually established based on the thermodynamic database of PC by introducing the unique reaction products of AAMs. The unique reaction products and their thermodynamic parameters are tabulated in Tables 1–4 for alkali-activated high-Ca system and alkali-activated low-Ca system.

Thermodynamic modelling of alkali-activated slag was initially conducted by using the thermodynamic database of PC. Altohough the modelling results can predict the phase composition evolution, it still needed experimental measurements to calibrate. With the established CNASH_ss model for describing C-(N-)A-S-H gel, thermodynamic modelling has been increasingly conducted to investigate the phase assemblage evolution of alkali-activated slag cements. Besides the phase evolution, thermodynamic modelling was also applied to predict the phase diagram, providing thretocal basis for the refined design of chemical properties of alkali-activated slag cement. In recent years, thermodynamic modelling tends to be used to investigate the durability of alkali-activated slag cements under single factor action such as carbonation, chloride attack and sulfate attack, as well as under multi-factors action, such as the combined attack by chloride and sulfate salts. Thermodynamic modelling has also been applied to predict the phase assemblage evolution of alkali-activated low- and medium-Ca systems. However, it is less applied as compared to those for alkali-activated high-Ca system. This is mainly due to the less developed thermodynamic database for alkali-activated low- and medium-Ca systems.

In addition to being used alone to study the phase assemblage evolution, thermodynamic modelling has also been coupled with other simulation techniques to numerically study AAMs. For instance, by coupling thermodynamic modelling and lattice Boltzmann method, a novel numerical model GeoMicro3D was developed to simulate the reaction process and microstructure formation of alkali-activated slag cement, with which the interaction mechanisms between chemical reaction, multi-ions transport and microstructure formation can be clarified. However, the numerical studies by coupling thermodynamic modelling and other simulation techniques are still limited for AAMs when compared to those for PC based materials.

Conclusions and Prospects Thermodynamic modelling show strong robustness in studying the phase evolution and durability performance of AAMs induced by chemical reactions. Firstly, thermodynamic modelling can predict the reaction products assemblage and pore solution composition of AAMs. Secondly, thermodynamic modelling can calculate the phase evolution of AAMs under the action of aggressive media, and then study the deteriation mechanism of AAMs. Finally, thermodynamic modelling can be combined with other numerical simulation techniques to study AAMs. At present, however, there are still some issues that need to be further studied:

1) The incomplete thermodynamic database for alkali-activated low-Ca system is an important reason for the limited thermodynamic modelling studies on alkali activated low and medium calcium systems. With the development of atomic- and molecular-scale simulation techniques, it is expected that a thermodynamic model describing the N-A-S-H gel can be established by *ab-initio* calculations and molecular dynamics simulations.

2) It is generally assumed that the amorphous phases in precursors are dissolved synchronously in current thermodynamic modelling of AAMs. However, the heterogeneous distribution of composition and structure of precursor makes this assumption in doubt. The non-uniformity of the dissolution of amorphous phases in precursor is an issue that needs to be further considered in future thermodynamic modelling studies.

3) The phase evolution of AAMs is actually a process coupling thermodynamics and kinetics. However, most of the thermodynamic modelling studies only focus on the phase assemblage at the equilibrium state, ignoring the kinetic issues before reaching the equilibrium. Considering the kinetic parameters such as dissolution rate and reaction rate etc. in thermodynamic modelling should be the focus of current and future thermodynamic modelling studies.

4) Phase evolution, microstructure damage and ions transport are three inter-dependent aspects for studying the durability performance of AAMs. However, the current thermodynamic modelling studies mainly focus on the phase evolution under the chemical attacks, while ignores the interaction between the phase evolution, microstructure damage and ions transport. In future studies, it is necessary to consider the interaction and establish the chemical-damage-transport model to numerically study the durability performance of AAMs.

Keywords alkali-activated materials; phase evolution; durability; thermodynamic database; thermodynamic modelling